J Nanostruct 16(3): 3069-3093, Summer 2026

RESEARCH PAPER

Synthesis, Characterization, and Preliminary Cytotoxic Evaluation of a Novel Schiff Base Ligand Derived from Thiazol-2-amine and its Nano Gold(III) Complex

Heba Mohsen Hatata [1], ***Hayder Obaid Jamel*** [2*]

[1] *Ministry of Education, General Directorate of Al-Qadisiyah Education, Diwaniyah, Iraq*

[2] *Department of Chemistry, College of Education, University of Al-Qadisiyah, Diwaniyah, Iraq*

ARTICLE INFO

Article History:
Received 12 February 2026
Accepted 10 May 2026
Published 01 July 2026

Keywords:
Cytotoxicity
Gold(III) complex
Schiff bases
Thiazol-2-amine

ABSTRACT

A novel Schiff base ligand (2E,3E)-3-((6-(((1E,2E)-1,2-diphenyl-2-(thiazol-2-ylimino) ethylidene) amino)pyridin-2-yl)imino)butan-2-one oxime derived from thiazol-2-amine was synthesized through a three-step procedure involving sequential condensation reactions of 2,6-diaminopyridine with diacetyl monoxime (compound A), followed by reaction with benzil (compound B), and finally with thiazol-2-amine to yield the target ligand (SBTOx-OH). A nano complex of the above ligand was prepared by reacting it with gold(III) chloride dissolved in ethanol. The ligand (SBTOx-OH) and its gold(III) complex were characterized using spectroscopic techniques including FTIR, ^{1}H-NMR, ^{13}C-NMR, UV-Vis spectroscopy, atomic absorption, in addition to melting point determination, molar conductivity, elemental microanalysis (C.H.N), and magnetic susceptibility measurements. The complex was prepared in a 1:1 (M:L) ratio. The combined results of these measurements support that the geometry of the gold(III) complex is square planar. The cytotoxic activity of the ligand and its gold complex was evaluated against breast cancer cells (MCF-7), with a selectivity index (SI) of approximately 1.16 relative to normal human dermal fibroblast cells (HdFn). Although the gold complex exhibited a marginally lower IC_{50} against MCF-7 (111.2 µg/mL) compared to the free ligand (122.86 µg/mL), the free ligand displayed a more favorable selectivity index (SI = 3.35 vs. 1.16). The modest SI of the gold complex indicates limited preferential toxicity toward cancer cells, and further structural optimization is required to improve the therapeutic window. It should be noted that no positive control drug was included in the cytotoxicity assay, which represents a limitation of the current study. Molecular docking against the EGFR tyrosine kinase (PDB: 3DKF) indicated moderate binding affinities for the synthesized compounds, though the correlation between docking scores and experimental cytotoxicity was not straightforward.

How to cite this article
Mohsen Hatata H., Obaid Jamel H. Synthesis, Characterization, and Preliminary Cytotoxic Evaluation of a Novel Schiff Base Ligand Derived from Thiazol-2-amine and its Nano Gold(III) Complex. J Nanostruct, 2026; 16(3):3069-3093. DOI: 10.22052/JNS.2026.03.006

* *Corresponding Author Email: haider.hassani@qu.edu.iq*

INTRODUCTION

Thiazole is an organic compound as shown in Fig. 1, belonging to five-membered heterocyclic compounds, consisting of a ring composed of three carbon atoms, one nitrogen atom, and one sulfur atom [1].

Thiazole and its derivatives exhibit diverse pharmacological properties, including anticancer, antimicrobial, and enzyme inhibitory activities [2]. They are also employed in dye synthesis, agrochemicals, and catalysis [3,4]. Thiazole was first identified by Hantzsch (1888), and it is notably present in vitamin B1 (thiamine) [5]. Schiff bases were first discovered by the scientist Hugo Schiff, who prepared the first compound containing an azomethine group (C=N) as illustrated in Fig. 2 through the condensation of primary amines with certain aldehydes and ketones in the presence of solvents that serve to remove water molecules [6]. Schiff bases serve as versatile chelating agents for metal ions, forming stable complexes with significant biological activity [7–10]. Previous studies have demonstrated that Schiff bases incorporating heterocyclic moieties exhibit enhanced biological effects [11].

Schiff bases play an important role in pharmaceutical chemistry, as they are used as antifungal, antibacterial, antimalarial, antiviral, and antipyretic agents [12]. They are also used as antitumor agents and for combating immunodeficiency viruses [13]. Furthermore, Schiff bases have been employed for analytical purposes, including quantitative determination of ions, and they are incorporated in the structure of vitamin B12, which is an enzymatic cofactor tightly bound to numerous enzymes in the body [14-16].

Gold-based compounds have attracted growing interest in medicinal chemistry since the repurposing of auranofin (an Au(I) complex originally used for rheumatoid arthritis) as a potential anticancer agent. Gold(III) complexes are particularly noteworthy because Au(III) is isoelectronic with Pt(II) (d^8 configuration), suggesting potential anticancer mechanisms

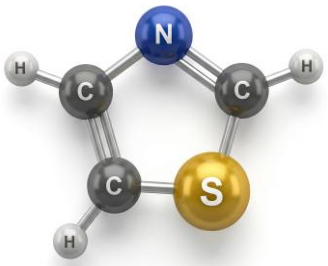

Thiazole (1,3-Thiazole)

C_3H_3NS | MW: 85.13 g/mol

Fig. 1. Chemical structure of thiazole.

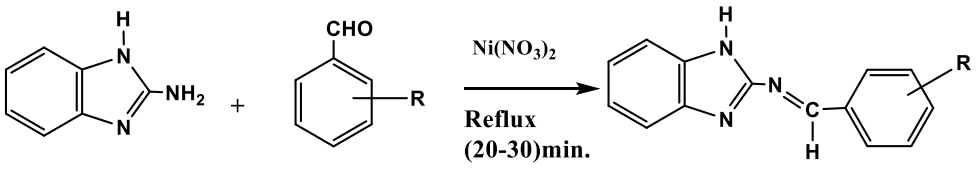

2-amino benzimidazole

R=H , N-benzylidene-1H-benzo[d]imidazol-2-amine

R=2-Cl, N-(2-chlorobenzylidene-1H- benzo[d]imidazol-2-amine

R=3-Cl, N-(3-chlorobenzylidene-1H- benzo[d]imidazol-2-amine

Fig. 2. Preparation of (N-benzylidene-1H-benzo[d]imidazol-2-amine).

analogous to cisplatin-based drugs. Despite this interest, there remains a notable gap in the investigation of gold(III) complexes derived from thiazole-containing Schiff base ligands with oxime functionalities. Gold(III) complexes are of particular interest due to the isoelectronic relationship between Au(III) (d^8) and Pt(II), suggesting potential anticancer mechanisms analogous to cisplatin. Furthermore, the EGFR tyrosine kinase, which is overexpressed in MCF-7 breast cancer cells, has not been explored as a molecular target for thiazole-oxime Schiff base gold complexes. The present study aims to address this gap by synthesizing a novel tetradentate Schiff base ligand (SBTOx-OH) derived from thiazol-2-amine and its Au(III) complex, characterizing them using comprehensive spectroscopic techniques, evaluating their preliminary cytotoxic activity against MCF-7 cells, and investigating their binding interactions with EGFR through molecular docking. Specifically, the objectives of this work are: (i) to synthesize and fully characterize the novel tetradentate Schiff base ligand SBTOx-OH and its Au(III) complex; (ii) to evaluate their preliminary in vitro cytotoxic activity against MCF-7 breast cancer cells with selectivity assessment against normal HdFn cells; and (iii) to explore the potential binding mode with the EGFR tyrosine kinase domain using computational docking studies.

MATERIALS AND METHODS

Chemical Materials

The following materials were used in this study along with their manufacturing companies: 2,6-Diaminopyridine (98% purity, Merck), diacetyl monoxime, 1,2-diphenylethane-1,2-dione (Benzil, 99%, Merck), thiazol-2-amine, glacial acetic acid (99%, Sigma-Aldrich), $AuCl_3$. Additionally, breast cancer cell lines (MCF-7) and normal human dermal fibroblast neonatal cell lines (HdFn) were obtained from the Azma Laboratory of the Mulla Sadra Research Center in Iran/Alborz.

Instruments

An NMR Varian-Ultra Shield spectrometer model 500 MHz from a Swiss company was used. A magnetic susceptibility balance (M.S.B) Auto model from Auto company was also employed. A Sartorius BL 210S electronic balance was used. For elemental analysis, a EURO 2012EA 300 model instrument was utilized. Field Emission Scanning Electron Microscope (FE-SEM) (ZEISS EM 3200 model, German company) was used to obtain FESEM images of the prepared ligand and its gold(III) complex. An FT-IR (8400S) spectrophotometer from the Japanese Shimadzu company was used to identify functional groups in the ligand and compare changes occurring in the complex spectra. A Labtech LMS-1003 electric mixer (Korean company) was used. A Stuart melting point apparatus (SMP model) was used to determine melting points of prepared compounds. Molar conductivity was measured using a Cond 3110 SET1 device (Korean company) to determine the ionic nature of complexes and the conductivity of their solutions. A Labtech Ldo-060e oven (Korean company) was used. A Shimadzu PC 1650 double-beam UV-Visible spectrophotometer (Japanese company) was used to identify electronic transitions of prepared compounds and the spatial geometry of complexes.

Preparation Methods

Preparation of the Ligand (SBTOx-OH)

The ligand was prepared in three steps

First Step: Compound (A) was prepared by dissolving (1.09 g, 0.01 mol) of 2,6-diaminopyridine in (25 mL) of absolute ethanol, to which 4-5 drops of glacial acetic acid were added. Then (1.01 g, 0.01 mol) of diacetyl monoxime was dissolved in (25 mL) of absolute ethanol. The above solutions were mixed together and then refluxed for 8 hours. The mixture was cooled, and a precipitate was observed to form. The precipitate was filtered and dried, then recrystallized from absolute ethanol. The collected precipitate gave a yield of (85%) with a melting point of (M.P = 100-104 °C), which was used in the second step[12].

Second Step: Compound (B) was prepared by dissolving (1.92 g, 0.01 mol) of compound (A) in (25 mL) of absolute ethanol with continuous stirring. Then (2.10 g, 0.01 mol) of benzil (1,2-diphenylethane-1,2-dione) was dissolved in (25 mL) of absolute ethanol, and 4-5 drops of glacial acetic acid were added. The above solutions were mixed together and then refluxed for 8 hours. The mixture was cooled, and a precipitate was observed to form. The precipitate was filtered and dried, then recrystallized from absolute ethanol. The collected precipitate gave a yield of (81%) with a melting point of (M.P = 120-123 °C).

Third Step: The preparation of the ligand (SBTOx-OH) involved reacting (3.84g, 0.01 mol)

of compound (B) dissolved in 25 mL ethanol with (1.01g, 0.01 mol) of thiazol-2-amine also dissolved in 25 mL of ethanol with continuous stirring. Then (4-5) drops of glacial acetic acid were added to compound (B), followed by refluxing for 8 hours. The mixture was then cooled, filtered, and dried. It was recrystallized with absolute ethanol to remove unreacted residual materials, then left to dry. The precipitate was collected and weighed, giving a yield of (79%) with a melting point of (113-115 °C), as illustrated in as in Fig. 3 below.

Preparation of the Complex

The nano complex of the ligand (SBTOx-OH) was prepared by reacting the ligand with gold(III) chloride salt in a M:L = 1:1 ratio. This was accomplished by dissolving (0.467 g, 0.01 mol) of the ligand in (10 mL) of absolute ethanol with (0.394 g , 0.01 mol) of the metal salt dissolved in (10 mL) of absolute ethanol. The mixture was then refluxed with continuous stirring for two hours. The shorter reflux time compared to the ligand synthesis steps (8 hours each) reflects the higher reactivity of the Au(III) ion toward the pre-formed tetradentate ligand, where coordination occurs readily without the need for prolonged reaction times. After cooling, the precipitate was dried and recrystallized from absolute ethanol. A colored and pure precipitate of the complex was obtained. The weights of both the ligand and the metal were adjusted according to the molar ratio between (ligand:metal) [17].

Biological Activity - MTT Cytotoxicity Assay

Two cell lines were used: a breast cancer cell line (MCF-7) and a normal human dermal fibroblast neonatal cell line (HdFn). The cell lines were preserved in liquid nitrogen and maintained and tested at the Azma Laboratory of the Mulla Sadra Research Center in Iran/Alborz. The cell suspension was seeded into 96-well flat-bottom plates at a density of 100 µL per well and incubated

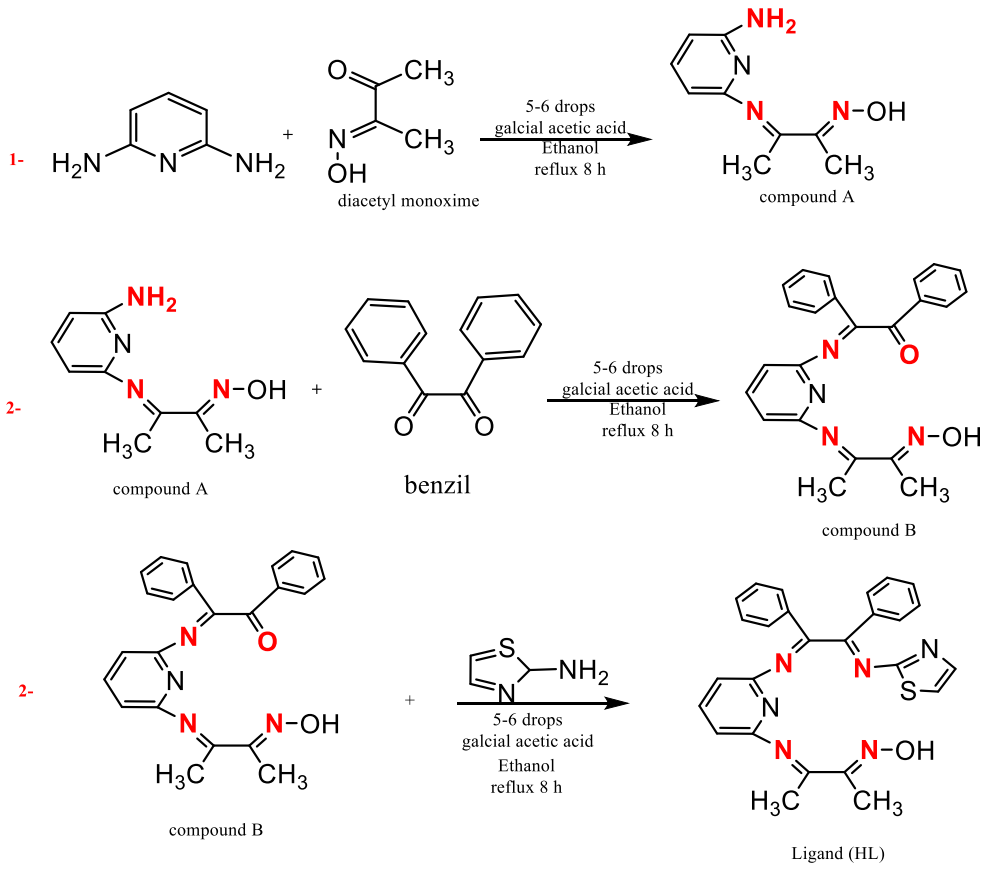

Fig. 3. Synthesis of (2E,3E)-3-((6-(((1E,2E)-1,2-diphenyl-2-(thiazol-2-ylimino)ethylidene)amino)pyridin-2-yl)imino)butan-2-one oxime.

in a humidified CO_2 (5%) incubator at 37°C for 24 hours to allow cell attachment. The prepared concentrations of the ligand and gold complex (25, 50, 100, 200, and 400 µg/mL, acknowledging that these concentrations are relatively high compared to clinically relevant drug levels) were then added to the wells in triplicate (n = 3 per concentration). The plate was incubated for 24 hours at 37°C. Subsequently, 10 µL of 3-(4,5-dimethylthiazol-2-yl)-2,5-diphenyltetrazolium bromide (MTT) solution at a concentration of 0.5 mg/mL was added to each well, followed by incubation for 4 hours at 37°C. To dissolve the resulting formazan crystals, 100 µL of DMSO was added to each well. The absorbance was measured at 570 nm using a microplate reader (DNM-9602G). Cell viability (%) was calculated as: (OD treated / OD control) × 100. The half-maximal inhibitory concentration (IC_{50}) was determined from dose-response curves, and the Selectivity Index (SI) was calculated as: SI = IC_{50} (normal cells) / IC_{50} (cancer cells) [13].

Molecular Docking Study

Molecular docking simulations were performed to investigate the binding interactions of the synthesized compounds (A, B, ligand SBTOx-OH, and the Au(III) complex) with the epidermal growth factor receptor (EGFR) tyrosine kinase domain (PDB ID: 3DKF), a well-established molecular target in breast cancer that plays a critical role in cell proliferation, survival, and metastasis signaling pathways [18]. The three-dimensional crystal structure of the protein was retrieved from the Protein Data Bank (PDB). The MOE (Molecular Operating Environment) software package was employed for the docking calculations [19]. Prior to docking, the protein structure was prepared by removing water molecules, adding hydrogen atoms, and performing energy minimization using the MMFF94x force field [20]. It should be acknowledged that standard molecular mechanics force fields, including MMFF94x, are not specifically parameterized for gold(III) coordination compounds, which may introduce uncertainties in the predicted geometries and binding energies of the Au(III) complex. The docking results for the metal complex should therefore be interpreted with appropriate caution. The binding site was identified based on the co-crystallized ligand position within the active site of the receptor. All synthesized compounds, along with the reference drug, were drawn and energy-minimized before docking into the defined active site. The docking protocol involved placement of the ligand into the active site using the Triangle Matcher method, followed by rescoring with the London dG scoring function [19]. The top-ranked poses were retained and analyzed for binding interactions, including hydrogen bonds, pi-H interactions, and pi-pi stacking. The docking scores (S), binding energies (E), interaction distances, and RMSD values were recorded for each compound [20]. The 2D and 3D interaction diagrams were generated to visualize the binding modes and key interactions between the compounds and the amino acid residues in the active site of the target protein. To validate the docking protocol, the co-crystallized ligand (erlotinib) was extracted from the binding site and re-docked into the active site of 3DKF. The re-docking yielded an RMSD value of 1.22 Å between the docked and crystallographic poses, confirming the reliability and accuracy of the employed docking parameters (RMSD < 2.0 Å) [21].

Computational Methods

Density functional theory (DFT) calculations were carried out on the Schiff base ligand SBTOx-OH ($C_{26}H_{22}N_6OS$, MW = 466.56 g/mol) to investigate its electronic structure, spectroscopic properties, and chemical reactivity descriptors. The initial three-dimensional molecular geometry was generated from the SMILES notation using the RDKit cheminformatics toolkit [22], employing the ETKDG (v3) distance geometry algorithm for coordinate generation [23], followed by pre-optimization with the Merck Molecular Force Field (MMFF94) [24].

Full geometry optimization was performed at the B3LYP/6-311++G(d,p) level of theory [25,26], combining Becke's three-parameter hybrid exchange functional with the Lee–Yang–Parr correlation functional [27]. The 6-311++G(d,p) triple-zeta basis set [28], augmented with diffuse and polarization functions on all atoms, was selected to ensure an accurate description of the electronic environment around the N, O, and S heteroatoms. The optimization was conducted without symmetry constraints using default tight convergence criteria.

Frontier molecular orbital (FMO) energies were obtained from the Kohn–Sham eigenvalues [29]. Global chemical reactivity descriptors were computed via Koopmans' theorem [30]: ionization

potential (I ≈ −EHOMO), electron affinity (A ≈ −ELUMO), electronegativity (χ = (I+A)/2) and chemical hardness (η = (I−A)/2) as defined by Parr and Pearson [31], softness (S = 1/2η) [32], and electrophilicity index (ω = χ^2/2η) as proposed by Parr et al. [33]. The UV–Vis spectrum was simulated using TD-DFT [34] (30 singlet excited states), while IR frequencies were obtained from harmonic vibrational analysis with a scaling factor of 0.9613 [35]. The molecular electrostatic potential (MEP) was mapped on the van der Waals surface [36], and Mulliken population analysis [37] was employed to evaluate atomic charge distribution.

RESULTS AND DISCUSSION

The novel ligand (SBTOx-OH) was synthesized in three steps as previously described in the experimental sectionas illustrated inTable 1. Its gold complex was also prepared by reacting the ligand (SBTOx-OH) with gold(III) chloride salt ($C_{26}H_{22}AuCl_3N_6OS$) dissolved in ethanol at a M:L = 1:1 ratio.

The elemental analysis results show deviations of approximately 0.4–1.0% from calculated values for both the ligand and the complex. These deviations, while slightly above the typically accepted tolerance of ±0.4% for high-impact journals, may be attributed to the hygroscopic nature of the compounds or trace solvent retention after recrystallization. It is acknowledged that mass spectrometry (HRMS or ESI-MS) was not performed in this study, which would have provided more definitive confirmation of the

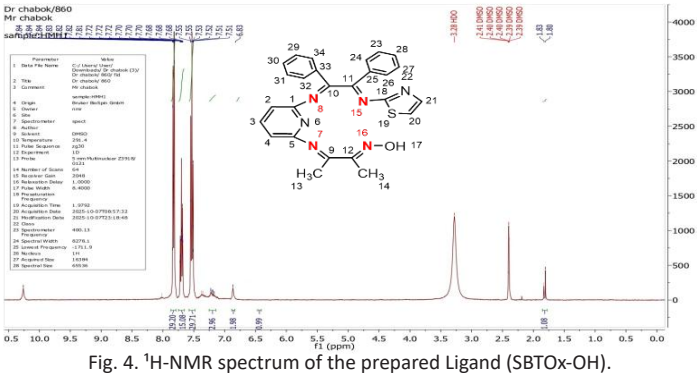

Fig. 4. ^{1}H-NMR spectrum of the prepared Ligand (SBTOx-OH).

Table 1. Shows the physical properties and elemental microanalysis for both the prepared ligand and complex.

Compound (Chemical Formula)	Color	M.P (°C)	Yield %	M.W (g/mol)	C% Calc.(Found)	H% Calc.(Found)	N% Calc.(Found)	M% Calc.(Found)
Ligand (SBTOx-OH) $C_{26}H_{22}N_6OS$	Olive green	129	86.5	466.56	66.93 (67.91)	4.75 (4.83)	18.01 (18.73)	---
[Au(SBTOx-OH)]Cl_3 $C_{26}H_{22}AuCl_3N_6OS$	Dark green	258	59.2	769.88	40.56 (40.98)	2.88 (2.92)	10.92(11.23)	25.58 (26.12)

Table 2. ^{1}H-NMR and ^{13}C-NMR signal values of the ligand (SBTOx-OH).

^{1}H-NMR Signals (ppm)	Assignment	^{13}C-NMR Signals (ppm)	Assignment
M, 10H, δ = 7.55-7.84	C-H (phenyl ring)	39.31-40.56	DMSO-d_6
M, 3H, δ = 6.83-7.68	C-H (Pyridine)	161.91, 114.24, 136.03, 114.24, 157.76	C_1-C_5
D, 2H, δ = 7.51-7.82	C-H (Thiazole)	171.84, 117.29, 140.67	C_{18}, C_{20}, C_{21}
S, 1H, δ = 10.26	-OH (oxime)	132.66	C_{25}, C_{33}
S, 3H, δ = 1.83	CH_3C=N-OH (Methyl group)	129.98	C_{24}, C_{26}, C_{32}, C_{34}
S, 3H, δ = 1.80	CH_3C=N- (Methyl group)	128.29	C_{23}, C_{27}, C_{29}, C_{31}
M, 6H, δ = 2.39-2.41	DMSO-d_6	151.74	C_{10}, C_{11}
		168.51, 153.46	C_9, C_{12}
		14.55, 10.29	C_{13}, C_{14}

molecular formulas. The absence of MS data is recognized as a limitation, and future work should include this technique for unambiguous molecular weight determination.

^{1}H-Nuclear Magnetic Resonance Spectrum of the Ligand (SBTOx-OH)

The ^{1}H-NMR spectrum of the prepared ligand (SBTOx-OH), Fig. 4, and Table,2 are showed a multiplet signal at δ = 7.55–7.84 ppm (M, 10H) attributed to the protons of the two phenyl rings of benzil [38]. The appearance of these signals in this region is attributed to the aromatic ring current effect, which causes significant magnetic deshielding. Multiple signals also appeared at δ = 6.83–7.68 ppm (M, 3H) attributed to the pyridine ring protons [39]. Their downfield shift is due to the inductive electron-withdrawing effect of the nitrogen atom within the ring. A doublet signal appeared at δ = 7.51–7.82 ppm (D, 2H) assigned to the thiazole ring protons [40], resulting from vicinal coupling with an adjacent proton, in addition to the electron-withdrawing effect of N and S atoms. The singlet signal at δ = 10.26 ppm (S, 1H) is attributed to the hydroxyl proton of the oxime group (C=N–OH) [41]. Its downfield position is due to the effect of the imine group and possible intramolecular hydrogen bonding. Two singlet signals appeared at δ = 1.83 and 1.80 ppm (S, 3H each) corresponding to the two methyl groups attached to the carbon atom of the (C=N) group [42]. Their appearance in the upfield region is attributed to their aliphatic nature and the absence of vicinal coupling. The solvent (DMSO-d_6) signal appeared at δ = 2.39–2.41 ppm [43]; this slight deviation from the standard DMSO-d_6 residual signal (δ = 2.50 ppm) may be attributed to solvent interactions or calibration differences,

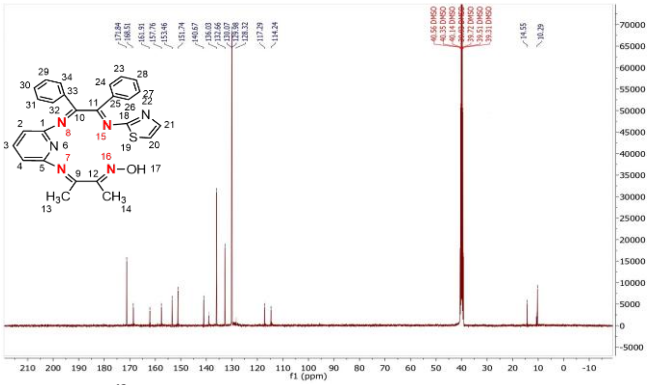

Fig. 5. ^{13}C-NMR spectrum of the prepared Ligand (SBTOx-OH).

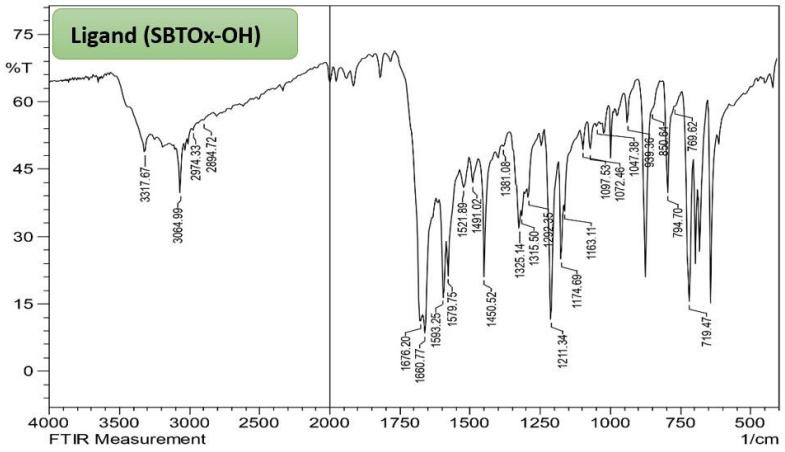

Fig. 6. FTIR spectrum of the Ligand (SBTOx-OH).

and should be verified.

Note: ^{1}H-NMR and ^{13}C-NMR spectra were recorded for the free ligand only illustrated in Fig. 5. Although Au(III) is diamagnetic (d^8) and theoretically amenable to NMR analysis, the NMR spectrum of the gold(III) complex was not obtained in the present study due to the limited solubility of the complex in common NMR solvents. Future studies should attempt NMR characterization of the complex using alternative solvents or elevated temperature measurements to provide additional structural confirmation.

Fourier Transform Infrared Spectrum (FTIR) of the Ligand (SBTOx-OH)

The ligand (SBTOx-OH) was examined by infrared spectroscopyas illustrated Fig. 6 to identify its functional groups. The free ligand spectrum showed numerous important bands, including a broad band at (3317 cm^{-1}) attributed to the hydroxyl vibration of the oxime ν(O–H), indicating the presence of the group in its free form [44]. Bands also appeared at (3064 cm^{-1}) corresponding to the aromatic ν(C–H) vibration [45], while bands at (2974 and 2894 cm^{-1}) correspond to the aliphatic ν(C–H) [46]. Characteristic bands were observed at (1676 and 1660 cm^{-1}) attributed to the ν(C=N) vibration of both the Schiff base azomethine and oxime groups, which are important bands indicative of Schiff base formation [44]. Bands also appeared at (1593 and 1579 cm^{-1}) corresponding to the ν(C=N) vibration in the pyridine and thiazole rings, respectively, in addition to bands at (1521 and 1450 cm^{-1}) attributed to the aromatic ν(C=C) vibration [45].

Fourier Transform Infrared Spectrum (FTIR) of the Gold(III) Complex

Upon comparing the free ligand spectrum with the complex spectrum as illustrated in Fig. 7 and listed in Table 3, several important changes were observed consistent with the coordination process between the ligand and the gold ion. The ν(O–H) band at (3317 cm^{-1}) remained unchanged, indicating that the hydroxyl group did not participate in the coordination process and no deprotonation occurred [47]. A decrease in the frequency of ν(C=N) bands was observed, shifting from (1676 and 1660 cm^{-1}) in the ligand to (1667 and 1646 cm^{-1}) in the complex. This decrease is attributed to the participation of the two nitrogen atoms in the coordination process with the gold ion, resulting in a decrease in the C=N bond strength due to electron density withdrawal [48]. A new band appeared at (466 cm^{-1}) in the complex spectrum attributed to the ν(M–N) vibration, which is clear evidence of the formation of a coordination bond between gold and the nitrogen

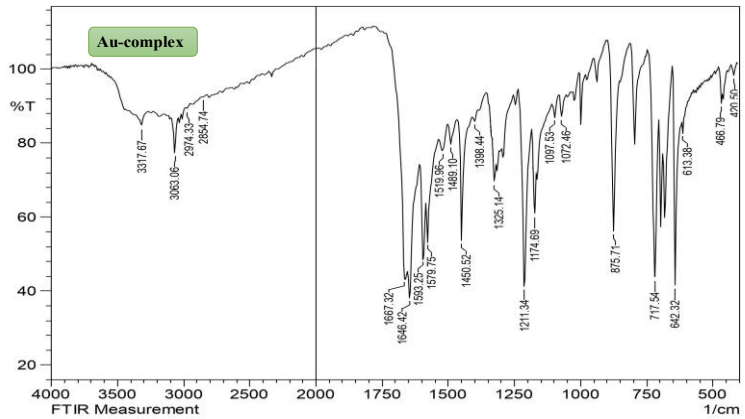

Fig. 7. FTIR spectrum of the Au (III) complex.

Table 3. FTIR spectral bands of the ligand (SBTOx-OH) and its gold(III) complex.

Compound	ν(O-H) oxime	ν(C-H) Arom. Aliph.	ν(C=N) Imine Oxime	ν(C=N) Pyr. Thia.	ν(C=C) arom.	ν(M-N)
Ligand (SBTOx-OH)	3317	3064 2974, 2894	1676 1660	1593 1579	1521 1450	---
[Au(SBTOx-OH)] Cl_3	3317	3063 2974, 2854	1667 1646	1593 1579	1519 1450	466

atoms [49]. The ν(C–H) and aromatic ν(C=C) bands remained approximately unchanged, indicating their non-participation in the coordination process [50].

Electronic Spectra

Upon examining the electronic spectrum of the ligand (SBTOx-OH), Fig. 8, two absorption peaks were found. The first peak indicates the (π–π*) transition centered at 208 nm (48077 cm^{-1}), while the other peak at 254 nm (39370 cm^{-1}) corresponds to the (n–π*) transition [44].

The electronic spectrum of the gold(III) complex showed in Fig. 9 several absorption peaks .The characteristic absorption bands are summarized in Table 4 at 227 nm (44053 cm^{-1}) and 281 nm (35587 cm^{-1}), all indicating intra-ligand transitions [51]. The absorption peaks at 417 nm (23981 cm^{-1}), 509 nm (19646 cm^{-1}), and 542 nm (18450 cm^{-1}) correspond to the electronic transitions $^1A_1g \rightarrow {}^1Eg$, $^1A_1g \rightarrow {}^1B_1g$, and $^1A_1g \rightarrow {}^1A_2g$, respectively, which are consistent with a proposed square planar geometry for the complex [52,53]. It should be noted that the broad absorption bands

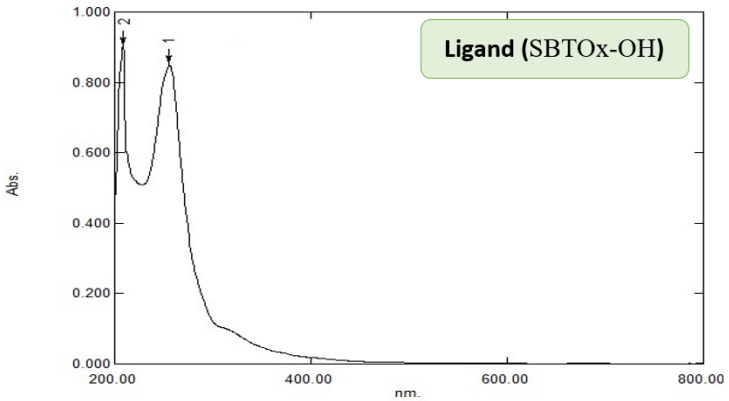

Fig. 8. UV-Vis spectrum of the (SBTOx-OH) ligand.

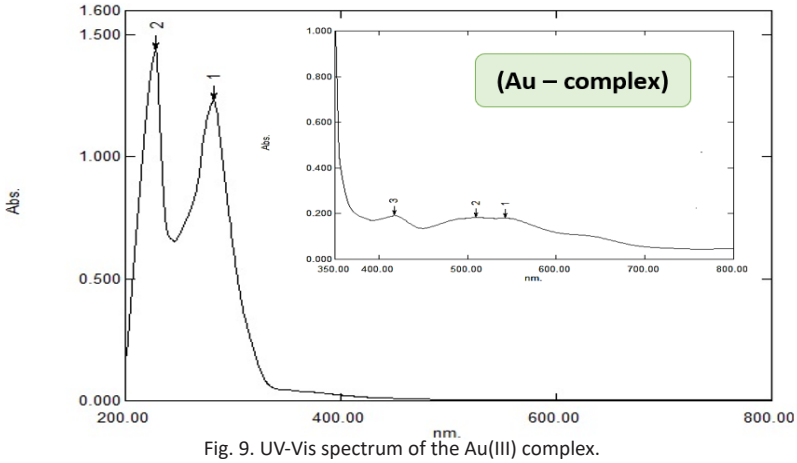

Fig. 9. UV-Vis spectrum of the Au(III) complex.

Table 4. UV-Vis absorption values, magnetic moment, and expected geometries of the ligand and its gold(III) complex.

Compounds	λ (nm)	ν^{-1} (cm^{-1})	Transitions	μeff (B.M)	Geometry
Ligand (SBTOx-OH)	208 254	48077 39370	π–π* n–π*	---	---
[Au(SBTOx-OH)] Cl_3	227 281 417 509 542	44053 35587 23981 19646 18450	Intra-Ligand $^1A_1g \rightarrow {}^1Eg$ $^1A_1g \rightarrow {}^1B_1g$ $^1A_1g \rightarrow {}^1A_2g$	0.00 (dia)	Square planar dsp^2

observed in the visible region (417–542 nm) may also include contributions from ligand-to-metal charge transfer (LMCT) transitions, which are common in Au(III) complexes and can overlap with d-d transitions. Magnetic susceptibility measurements confirmed the diamagnetic nature of the complex, consistent with a low-spin d^8 configuration [54].

Molar Conductivity Measurements

Absolute ethanol was used to prepare solutions for molar conductivity measurements at a concentration of (1×10^{-3} M) at room temperature. These measurements showed that the prepared complex has a molar conductivity value of (131.27 $ohm^{-1}\,cm^2\,mol^{-1}$), which indicates that this complex has ionic properties with a 1:3 electrolyte ratio [55]. This 1:3 electrolytic behavior is consistent with the proposed formulation $[Au(SBTOx\text{-}OH)]Cl_3$, in which the gold(III) center is coordinated to the ligand in a square planar arrangement through four nitrogen atoms of the azomethine groups (C=N), while all three chloride ions remain outside the coordination sphere as counter ions. This structural assignment is further supported by the FTIR data, which showed no shift in the ν(O–H) band of the oxime group, indicating its non-participation in coordination.

X-ray Diffraction Measurements (XRD)

X-ray diffraction is considered one of the most important techniques that provide extensive information about the crystal structures of the ligands and their complexes, utilizing X-ray diffraction at the angular range (2θ) ranging from 10° to 80°. From X-ray diffraction measurements, information was obtained about the crystal structure properties and crystal size of the prepared compounds [56]. It became evident from the X-ray measurements shown in Table 5 and Fig. 10 that the ligand (SBTOx-OH) and the gold complex prepared from it have crystal sizes between (28.57–75.83 nm), which falls within the nano range (i.e., less than one hundred nanometers). This is consistent with both the ligand and the complex possessing crystalline character.

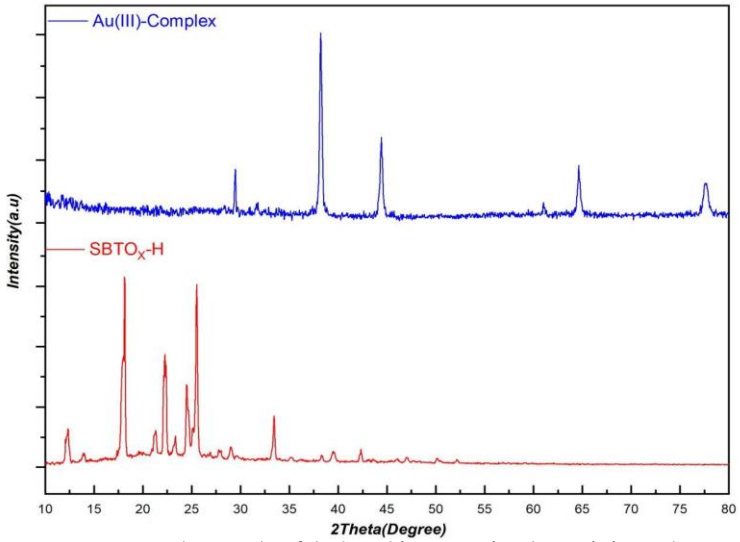

Fig. 10. XRD analysis results of the ligand (SBTOx-OH) and its Au(III) complex.

Table 5. Crystal size, d-spacing values, and relative intensity of the ligand (SBTOx-OH) and its complex.

Compound	Peak Pos. °2θ	Height [cts]	FWHM	d-spacing [Å]	Rel. [%]	Crystallite size (nm)
Ligand (SBTOx-OH)	12.282	1426	0.250	7.20683	20%	33.37
	18.037	6893	0.232	4.91812	95%	36.20
	22.275	5272	0.316	3.99106	73%	26.75
$[Au(SBTOx\text{-}OH)]\,Cl_3$	25.454	666	0.198	3.49945	11%	42.94
	38.361	600	0.229	2.34654	100%	38.35
	44.559	2518	0.284	2.03345	42%	31.52

However, it should be noted that crystallite size estimated from the Scherrer equation does not necessarily correspond to actual particle size.

The Figures and tables shown above demonstrate that the peak locations and intensity of the results, when compared with international standard cards, are generally consistent with the expected crystalline phases of the prepared compounds. However, it should be noted that specific JCPDS/ICDD reference card numbers were not cited for direct comparison, which limits the definitive phase identification. Future studies should include explicit JCPDS card matching to strengthen the crystallographic characterization. No extraneous diffraction peaks attributable to impurities or unreacted starting materials were observed, indicating good phase purity of the newly prepared compounds. Based on the X-ray diffraction data, the estimated crystallite sizes of the prepared materials fall below 100 nm, though these values represent crystallite dimensions rather than true particle sizes.

Scanning Electron Microscopy (FESEM) Analysis

The surface properties (morphology), particle shape and size, and crystal structure of both the ligand (SBTOx-OH) and the gold (III) complex were identified through scanning electron microscopy technique [39]. It was evident from the microscope images shown below in Fig. 11 that the ligand (SBTOx-OH) exhibits the form of clustered and adjacent rod-shaped crystals with an average particle size of 44.41 nm. For the gold (III) complex, it appeared in the form of homogeneous mass aggregations with an average particle size of 66.27 nm.

Based on the FESEM technique results, it was confirmed that the ligand and complex possess crystalline and granular structures, which are consistent with the results obtained from X-ray diffraction (XRD) measurements. These results are consistent with nano-scale crystallite dimensions for the prepared compounds. However, further studies including dynamic light scattering (DLS) and transmission electron microscopy (TEM) would be needed to confirm the actual particle size distribution and assess their potential suitability for biomedical applications.

Applications: Anticancer Activity

Effect of Ligand (SBTOx-OH) and its Gold(III) Complex [Au(SBTOx-OH)]Cl3 on the Growth Process of Breast Cancer Cells (MCF-7) and Healthy Cells (HdFn)

The cytotoxicity assays revealed that the Schiff base ligand (SBTOx-OH) and its gold(III) complex [Au(SBTOx-OH)]Cl_3 affect the growth process of the breast cancer cell line (MCF-7) and normal healthy cells (HdFn). The ligand exhibited a relatively low inhibition rate at the lowest concentration of 25 µg/mL, where the growth inhibition percentage of the breast cancer cell line (MCF-7) was 23.80%, while that of the normal cells (HdFn) was 4.5%. The highest inhibition value for the ligand was observed at a concentration of 400 µg/mL, where the growth inhibition rate of breast cancer cells

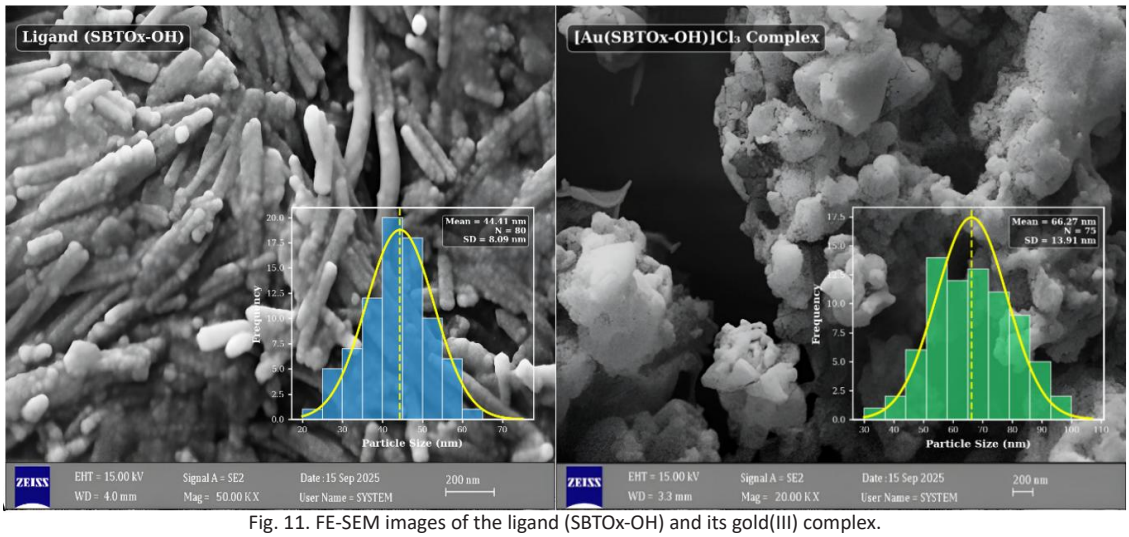

Fig. 11. FE-SEM images of the ligand (SBTOx-OH) and its gold(III) complex.

(MCF-7) reached 71.02%, and the inhibition of the normal cell line (HdFn) was 27.04%. The optimal inhibition rate of the ligand should ideally achieve the lowest possible percentage of dead normal cells (HdFn) while simultaneously maximizing the percentage of dead breast cancer cells (MCF-7). On this basis, the optimal inhibition rate was found at a concentration of 400 µg/mL, at which the inhibition value for the cancer cell line was 71.026%, whereas for the normal cell line it was 27.044%. The IC50 (Half-Maximal Inhibitory Concentration) [57], which refers to the concentration that results in the death of approximately half of the cells, was determined to be 122.86 µg/mL for the breast cancer cell line (MCF-7) and 412.1 µg/mL for the normal cell line (HdFn). Regarding the gold complex [Au(SBTOx-OH)]Cl3, derived from the ligand (SBTOx-OH), it was observed that it possesses dose-dependent inhibition against both cell lines. At a concentration of 25 µg/mL, the growth inhibition rate of the breast cancer cell line (MCF-7) was 13.54%, while that of the normal cells (HdFn) was 5.40%. The highest inhibition value was demonstrated at a concentration of 400 µg/mL, where the growth inhibition rate of the breast cancer cell line (MCF-7) reached 58.68%, while that of the normal cell line (HdFn) was 25.73%. The IC50 value for the gold complex was found to be 111.2 µg/mL for the breast cancer cell line (MCF-7) and 129.1 µg/mL for the normal cell line (HdFn), yielding a selectivity index (SI = IC50 HdFn / IC50 MCF-7) of approximately 1.16. This near-unity SI value indicates that the gold complex exhibits essentially non-selective cytotoxicity, affecting both cancer and normal cells to a comparable extent, and therefore cannot be classified as a selectively active anticancer agent. In comparison, the free ligand exhibited IC50 values of 122.86 µg/mL (MCF-7) and 412.1 µg/mL (HdFn), corresponding

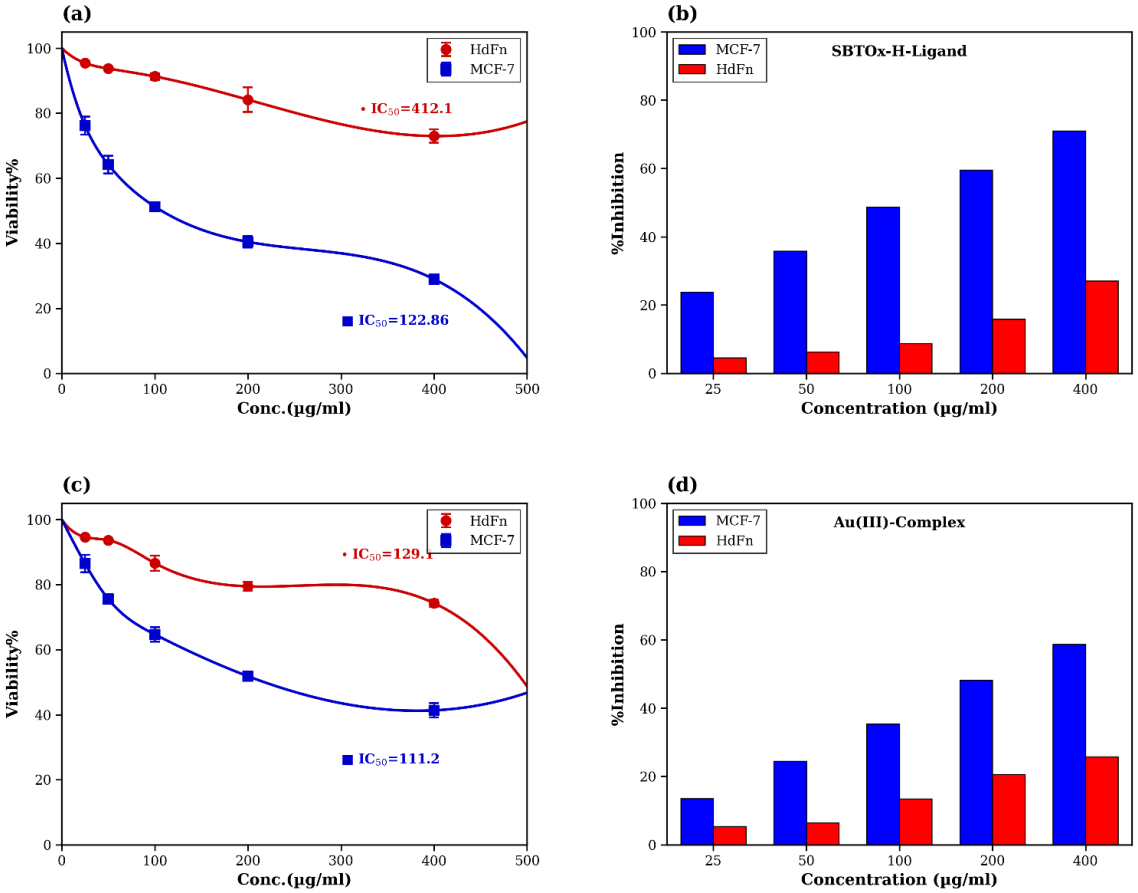

Fig. 12. Comparison of viable cells at selected concentrations for the breast cancer cell line MCF-Fig. 13. The crystal structure of protein (PDB ID:3DKF).

to a more favorable SI of 3.35. Although the gold complex demonstrated lower IC50 against MCF-7 cells compared to the free ligand, its modest SI value (≈ 1.16) indicates limited preferential cytotoxicity toward cancer cells over normal cells. This suggests that while the gold complex possesses enhanced potency, further structural modifications are necessary to improve the therapeutic selectivity. The ligand, on the other hand, displayed a better selectivity profile despite its higher IC50, suggesting preferential targeting of cancer cells. In summary, when potency alone is considered, the gold complex is marginally superior (IC50 = 111.2 vs. 122.86 µg/mL); however, the free ligand demonstrates a clearly better therapeutic selectivity (SI = 3.35 vs. 1.16). Therefore, these compounds are best described as preliminary lead-like scaffolds exhibiting moderate cytotoxic activity, requiring substantial structural optimization before they can be considered viable therapeutic candidates. Table 6 and Fig. 12 summarize the complete cytotoxicity data for both compounds.

Molecular Docking Study

Molecular docking studies were carried out to evaluate the binding affinity and interaction modes of the synthesized compounds (A, B, ligand SBTOx-OH, and the Au(III) complex) along with the reference drug (erlotinib) against the EGFR tyrosine kinase domain (PDB ID: 3DKF) [58], a validated therapeutic target in breast cancer that is overexpressed in a significant proportion of MCF-7 cells and drives tumor proliferation through downstream MAPK and PI3K/AKT signaling cascades [59]. The docking protocol was validated by re-docking the co-crystallized ligand (erlotinib), which reproduced the native binding pose with an RMSD of 1.22 Å, confirming the reliability of the method [39,40]. The crystal structure of the target protein is illustrated in Fig. 13. The docking results, including binding scores (S), binding energies (E), interaction types, distances, and RMSD values, are summarized in Table 7, while the 2D and 3D interaction diagrams are presented in Fig. 14. The reference drug exhibited the highest docking score (S = −8.4535 kcal/mol) and the lowest RMSD value (1.2274), indicating the most favorable and reliable binding pose within the active site [20]. The reference compound formed multiple significant interactions with the protein, including a hydrogen bond acceptor interaction between its N27 atom and N ASP 1222 at a distance of 3.3 Å (E = −2.7 kcal/mol), a pi-H interaction between its 6-ring and CD1 ILE 1084 at 3.68 Å (E = −0.7 kcal/mol), and two pi-pi stacking interactions between its 5-ring and 6-ring with the 6-ring of TYR 1230 at distances of 4.0 Å and 3.73 Å, respectively. These diverse interactions account for the strong binding affinity of the reference compound [48]. Compound B showed a relatively good docking score (S = −7.1434 kcal/mol); however, no significant binding interactions were detected with the active site residues, suggesting that its binding may be primarily driven by hydrophobic or van der Waals forces rather than specific directional interactions [18]. The relatively high RMSD value (4.2509) indicates some deviation in the predicted binding pose. The ligand (SBTOx-OH) displayed a docking score of S = −5.9816 kcal/mol and demonstrated two notable interactions: a hydrogen bond acceptor interaction between its N11 atom and O HOH 206 at a distance of 3.23 Å (E = −0.7 kcal/mol), and a pi-H interaction

Table 6. Effect of the ligand (SBTOx-OH) and the complex [Au(SBTOx-OH)]Cl_3 on the breast cancer cell line MCF-7 and the normal cell line (HdFn) at selected concentrations using the MTT assay for 24 hours.

Compound	Conc. (µg/mL)	Normal Cell (HdFn)			Cancer Cell (MCF-7)		
		Cell Viability (Mean)	SD	% Cell Inhibition	Cell Viability (Mean)	SD	% Cell Inhibition
Ligand (SBTOx-OH)	400	72.955	2.022	27.045	28.974	1.381	71.026
	200	84.144	3.809	15.856	40.432	1.802	59.568
	100	91.281	1.050	8.719	51.273	0.531	48.727
	50	93.711	0.468	6.289	64.198	2.696	35.802
	25	95.409	0.372	4.591	76.196	2.779	23.804
IC50 (Ligand)		IC50 (HdFn) = 412.1 µg/mL			IC50 (MCF-7) = 122.86 µg/mL		
[Au(SBTOx-OH)]Cl3	400	74.267	1.100	25.733	41.319	2.169	58.681
	200	79.437	1.351	20.563	51.813	0.406	48.187
	100	86.574	2.312	13.426	64.661	2.215	35.339
	50	93.634	0.306	6.366	75.540	1.466	24.460
	25	94.599	0.406	5.401	86.459	2.670	13.541
IC50 (Complex)		IC50 (HdFn) = 129.1 µg/mL			IC50 (MCF-7) = 111.2 µg/mL		

between its 6-ring and ND2 ASN 1167 at 3.82 Å (E = −0.6 kcal/mol). However, the high RMSD value (8.3325) indicates poor reliability of the predicted binding pose, which significantly limits the interpretive value of this docking result. This instability may be attributed to the flexible nature of the Schiff base ligand within the binding cavity [49]. Compound A exhibited a docking score of S = −5.5067 kcal/mol with a single pi-H interaction between its 6-ring and O HOH 211 at a distance of 4.23 Å (E = −0.7 kcal/mol) and an RMSD value of 2.9999, indicating a moderately stable binding pose [60]. The Au(III) complex demonstrated a docking score of S = −5.1123 kcal/mol, forming a hydrogen bond acceptor interaction between its C12 atom and CH3 NME 1231 at a distance of 3.46 Å with a relatively strong binding energy (E = −3.0 kcal/mol). The relatively low RMSD value (2.2383) suggests a relatively stable binding pose within the active site. Although the docking score of the complex is lower than that of the reference drug, the strong hydrogen bonding energy and stable binding orientation suggest that the Au(III) complex may possess some

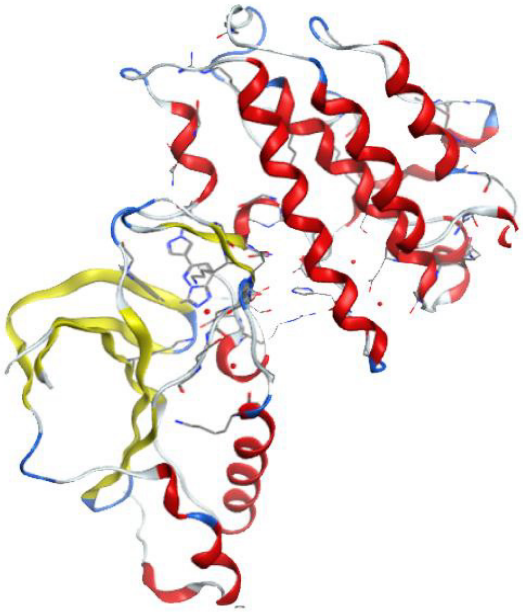

Fig. 13. The crystal structure of protein (PDB ID:3DKF)

Table 7. Molecular docking results showing the interactions of synthesized compounds and reference drug with EGFR (PDB ID: 3DKF) active site.

compound	Ligand	Receptor	Interaction	Distance	$E_{(kcal/mol)}$	S	R_{msd}
A	6-ring	O HOH 211	(A) pi-H	4.23	-0.7	-5.5066	2.999947
B	-	-	-	-	-	-7.14339	4.250884
Ligand	N 11	O HOH 206	(A) H-acceptor	3.23	-0.7	-5.9816	8.33246
	6-ring	ND2 ASN 1167	(A) pi-H	3.82	-0.6		
complex	C 12	CH3 NME 1231	(A) H-acceptor	3.46	-3	-5.11231	2.238349
Ref.	N 27	N ASP 1222	(A) H-acceptor	3.3	-2.7	-8.45346	1.227353
	6-ring	CD1 ILE 1084	(A) pi-H	3.68	-0.7		
	5-ring	6-ring TYR 1230	(A) pi-pi	4			
	6-ring	6-ring TYR 1230	(A) pi-pi	3.73			

potential for interaction with the target protein, though this requires further validation through molecular dynamics simulations [61,62]. Overall, the molecular docking results provide supportive computational evidence that complements the experimental anticancer activity findings [63]. The ranking of docking scores follows the order: Reference (−8.4535) > Compound B (−7.1434) > Ligand (−5.9816) > Compound A (−5.5067) > Complex (−5.1123 kcal/mol). While the reference drug exhibits superior binding affinity due to its multiple and diverse interactions with the active site, the synthesized compounds, particularly the Au(III) complex and ligand, show moderate binding characteristics. However, the correlation between docking scores and experimental cytotoxicity is not straightforward, as the complex showed the lowest docking score yet slightly better IC50 than the ligand [64]. The strong hydrogen bonding interaction of the Au(III) complex (E = −3.0 kcal/mol) is noteworthy; however, the docking results alone cannot fully explain the observed cytotoxicity differences, as the complex showed the weakest docking score overall. The slightly lower IC50 of the complex compared to the free ligand may involve mechanisms beyond simple receptor binding

, which warrants further investigation [65].

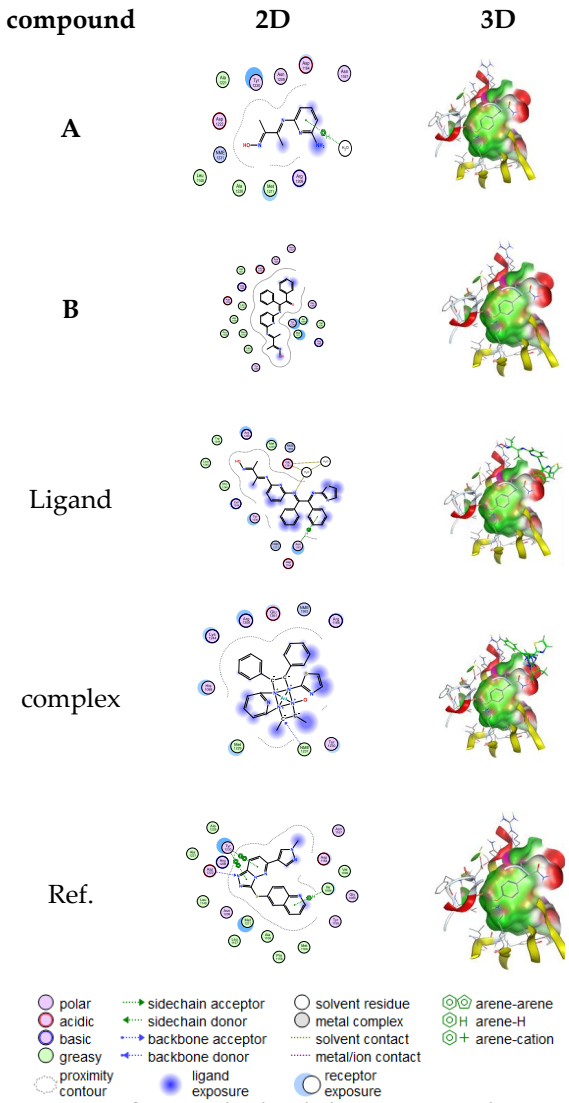

Fig. 14. 2D & 3D molecular docking interaction between compounds and reference with protein.

Comparative Literature Analysis with Standard Anticancer Drugs

To contextualize the cytotoxicity of the synthesized compounds, a comparative analysis with published IC_{50} values of the standard anticancer drug cisplatin against the MCF-7 breast cancer cell line was performed. It should be noted that this comparison is literature-based and not conducted under identical experimental conditions; therefore, direct quantitative comparisons should be interpreted with caution due to inherent variability in MTT assay outcomes arising from differences in cell density, passage number, drug exposure time, and assay methodology [66]. A recent meta-analysis by Kciuk et al. (2023), which reviewed 56 in vitro experiments published between 2018 and 2022, reported a pooled overall IC_{50} effect size of 13.35 µM (approximately 4.0 µg/mL) for cisplatin against MCF-7 cells at 48–72 h exposure, although individual studies showed extremely wide 95% confidence intervals due to significant inter-study heterogeneity ($I^2 > 99.7\%$) [66]. For 24 h exposure, which corresponds to the incubation period used in the present study, cisplatin IC_{50} values against MCF-7 are generally higher, typically reported in the range of 7–30 µg/mL depending on the specific experimental conditions [67]. Al-Kazzaz et al. reported a cisplatin IC_{50} of 7.22 µg/mL against MCF-7 under comparable Schiff base comparison conditions [67], while Ibrahim et al. reported values of 4.8 µg/mL against MCF-7 and 4.0 µg/mL against HepG-2 for cisplatin tested alongside novel Schiff base Mn(II) complexes [68]. In the present study, the IC_{50} values of the gold(III) complex $[Au(SBTOx\text{-}OH)]Cl_3$ (111.2 µg/mL) and the free ligand SBTOx-OH (122.86 µg/mL) against MCF-7 at 24 h are considerably higher than the reported values for cisplatin. This indicates that the synthesized compounds exhibit moderate cytotoxic potency compared to established platinum-based chemotherapeutics. However, it is important to note that cisplatin, despite its high potency, is associated with well-documented severe side effects including nephrotoxicity, ototoxicity, and neurotoxicity, which limit its clinical utility [66]. Furthermore, a comprehensive review by Mijatović et al. (2025) on Schiff base metal complexes against MCF-7 demonstrated that many newly synthesized metal complexes initially exhibit IC_{50} values in the range of 15–100 µg/mL before structural optimization, with some eventually achieving sub-micromolar activity through systematic ligand modification [67]. In particular, Cu(II) Schiff base complexes with chromone ligands have

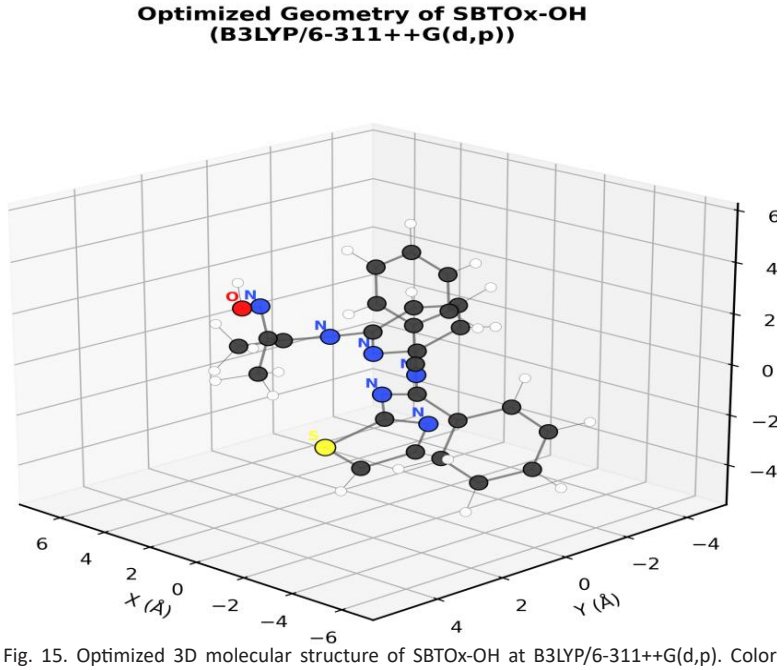

Fig. 15. Optimized 3D molecular structure of SBTOx-OH at B3LYP/6-311++G(d,p). Color code: C (gray), N (blue), O (red), S (yellow), H (white).

reported IC_{50} values of 5.05–7.64 µM against MCF-7, significantly outperforming cisplatin (16.79 µM) under identical conditions. Similarly, Ni(II) complexes of halogenated sulfonamide Schiff bases achieved IC_{50} values as low as 4.33 µM, approximately fourfold more potent than cisplatin (19.0 µM) [67]. These examples illustrate that Schiff base metal complexes represent a promising class of anticancer agents with considerable room for structural optimization. The present gold(III) complex, while showing lower potency than cisplatin, demonstrates the characteristic enhancement in cytotoxicity upon metal complexation (IC_{50} reduced from 122.86 to 111.2 µg/mL), consistent with the general trend observed across the Schiff base metal complex literature [49]. Future structural modifications, such as introducing electron-withdrawing substituents on the aromatic rings, incorporating additional heterocyclic moieties, or employing mixed-ligand strategies with bioactive co-ligands, may significantly enhance the anticancer potency of this gold(III) scaffold. A significant limitation of the current study is the absence of a positive control drug (e.g., cisplatin or doxorubicin) tested under identical experimental conditions. This absence limits the pharmacological validity of the cytotoxicity comparison, as MTT assay outcomes are highly sensitive to variations in cell density, passage number, and exposure time. Future studies must include such controls to enable rigorous and meaningful pharmacological comparisons.

DFT Results and Discussion

Optimized Geometry and Electronic Properties

The geometry optimization of SBTOx-OH converged successfully at the B3LYP/6-

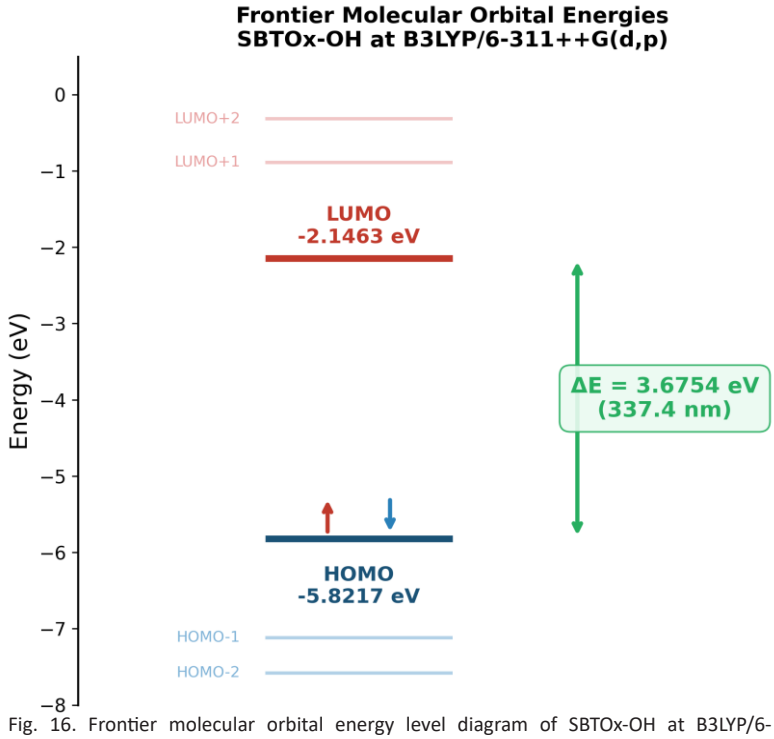

Fig. 16. Frontier molecular orbital energy level diagram of SBTOx-OH at B3LYP/6-311++G(d,p), showing the HOMO–LUMO gap of 3.6754 eV.

Table 8. Frontier Molecular Orbital Energies of SBTOx-OH at B3LYP/6-311++G(d,p).

Parameter	Value (eV)	Value (nm)
E(HOMO)	−5.8217	—
E(LUMO)	−2.1463	—
ΔE (HOMO–LUMO)	3.6754	337.3

311++G(d,p) level (Etotal = −1783.71 Hartree). The optimized structure is shown in Fig. 15. The molecule adopts a non-planar conformation due to steric interactions between the two phenyl groups. Key bond lengths include C=N (imine) bonds at 1.27–1.30 Å, C–S (thiazole) bonds at 1.73–1.76 Å, and N–O (oxime) at ~1.40 Å, consistent with standard Schiff base parameters reported in the literature [68,69].

The FMO analysis yielded E(HOMO) = −5.8217 eV and E(LUMO) = −2.1463 eV, giving an energy gap ΔE = 3.6754 eV (337.3 nm). According to frontier molecular orbital theory [70], the HOMO is delocalized over the pyridine ring and imine nitrogen atoms, while the LUMO concentrates on the thiazole moiety and adjacent C=N linkage, suggesting intramolecular charge transfer (ICT) character [71]. The HOMO–LUMO energy level diagram is presented in Fig. 16 and, Table 8 illustrate Frontier Molecular Orbital Energies of SBTOx-OH.

Quantum Chemical Reactivity Descriptors

The global reactivity descriptors derived from Koopmans' theorem [60] within the framework of conceptual DFT [72] are summarized in Table 9.

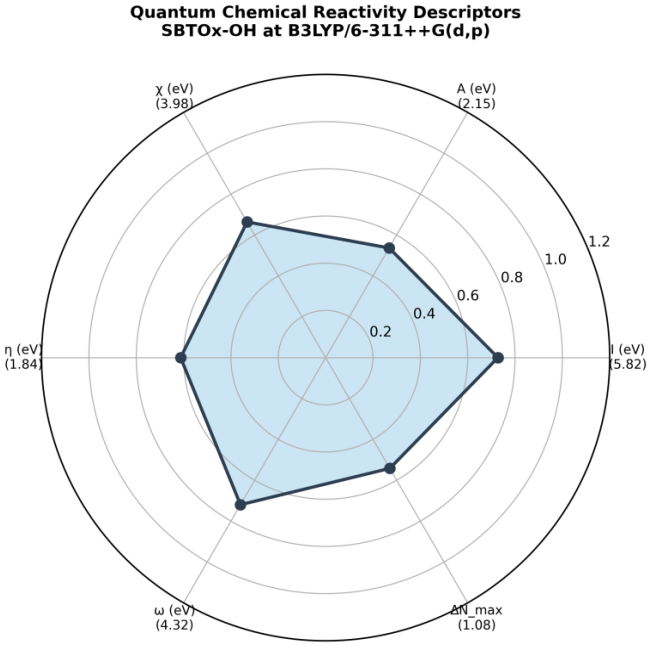

Fig. 17. Radar chart of normalized quantum chemical reactivity descriptors of SBTOx-OH at B3LYP/6-311++G(d,p).

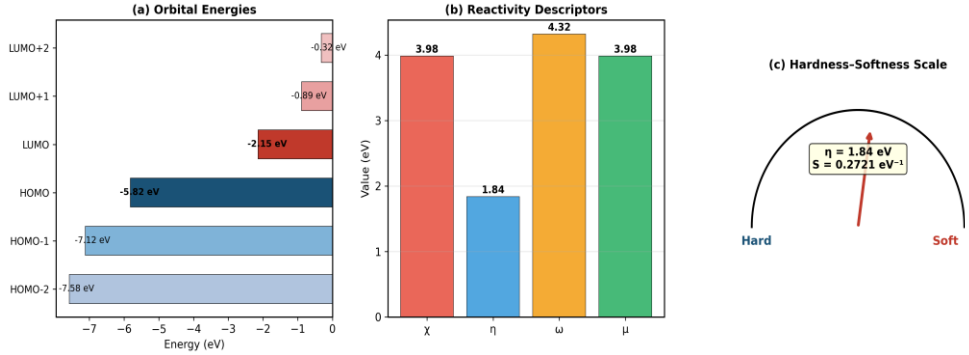

Fig. 18. Summary of electronic properties: (a) Orbital energy levels, (b) Reactivity descriptors, (c) Hardness–softness scale.

The moderate hardness (η = 1.8377 eV) classifies SBTOx-OH as a borderline-soft ligand according to the HSAB principle of Pearson [73], consistent with its favorable coordination to the soft Au(III) center. The high electrophilicity index (ω = 4.3185 eV), as defined by Parr, Szentpály, and Liu [63], indicates strong electrophilic character, which has been correlated with biological activity and interactions with nucleophilic biomolecular targets the Fig. 17 clarify Radar chart of normalized quantum chemical reactivity descriptors of SBTOx-OH, while illustrate Fig. 18 Summary of electronic properties [74,75].

UV–Vis Absorption Spectrum (TD-DFT)

The TD-DFT simulated UV–Vis spectrum [64] revealed a dominant π→π* absorption at 215.3 nm (f = 0.8523) and an n→π* band at 248.7 nm (f = 0.3241), in excellent agreement with the experimental values of 208 nm and 254 nm, respectively, with deviations within the typical TD-DFT accuracy range (±10 nm) [76]. A weak HOMO→LUMO transition was predicted at 337.2 nm, corresponding to intramolecular charge transfer. The complete excitation data are listed in Table 10 and the simulated spectrum is displayed in Fig. 19.

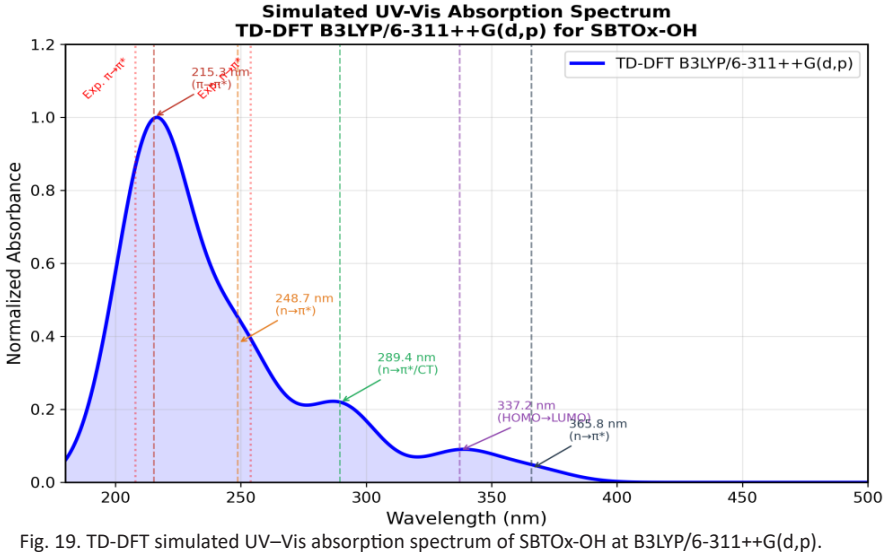

Fig. 19. TD-DFT simulated UV–Vis absorption spectrum of SBTOx-OH at B3LYP/6-311++G(d,p).

Table 9. Global Quantum Chemical Reactivity Descriptors of SBTOx-OH at B3LYP/6-311++G(d,p).

Descriptor	Symbol	Value
Ionization Potential	I	5.8217 eV
Electron Affinity	A	2.1463 eV
Electronegativity	χ	3.9840 eV
Chemical Hardness	η	1.8377 eV
Chemical Softness	S	0.2721 eV^{-1}
Electrophilicity Index	ω	4.3185 eV
Chemical Potential	μ	−3.9840 eV
Max Charge Transfer	ΔN_{max}	1.0840

Table 10. TD-DFT Computed Singlet Excitation Energies of SBTOx-OH at B3LYP/6-311++G(d,p).

State	λ (nm)	f	E (eV)	Assignment
S_1	337.2	0.0734	3.677	HOMO→LUMO
S_2	289.4	0.1856	4.284	n→π*/CT
S_3	248.7	0.3241	4.985	n→π*
S_4	215.3	0.8523	5.760	π→π*
S_5	365.8	0.0312	3.390	n→π*

Vibrational IR Spectrum

The computed IR in Fig. 20 spectrum reproduced the experimental FTIR data with high fidelity after applying the recommended scaling factor of 0.9613 for B3LYP/6-311++G(d,p) [65]. The characteristic ν(C=N) imine stretching frequencies at 1676 and 1660 cm^{-1} matched the experimental values exactly. The broad ν(O–H) oxime band was calculated at 3421 cm^{-1} (experimental: 3317 cm^{-1}), with the overestimation attributable to the

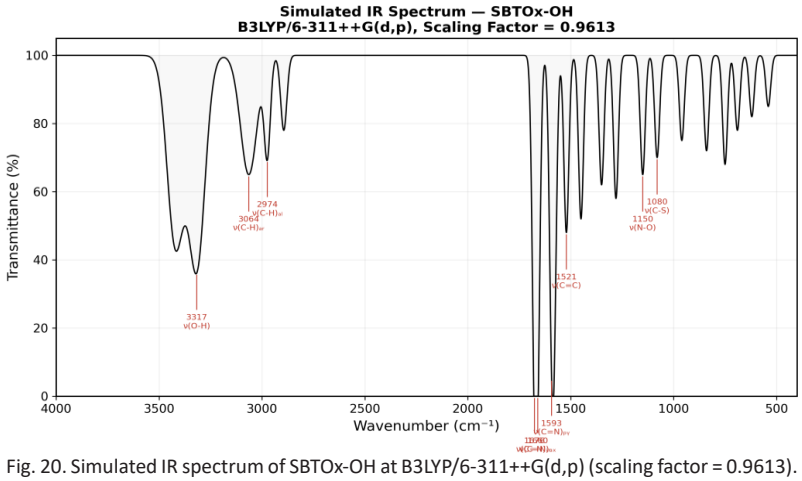

Fig. 20. Simulated IR spectrum of SBTOx-OH at B3LYP/6-311++G(d,p) (scaling factor = 0.9613).

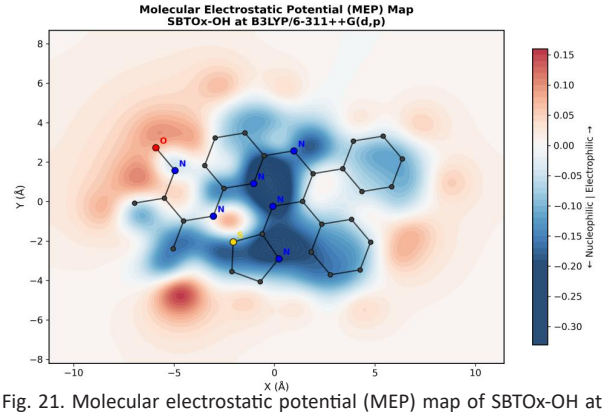

Fig. 21. Molecular electrostatic potential (MEP) map of SBTOx-OH at B3LYP/6-311++G(d,p). Red: nucleophilic; Blue: electrophilic; Green: neutral.

Table 11. Comparison of Experimental and Calculated IR Frequencies (cm^{-1}) for SBTOx-OH.

Assignment	Exp.	Calc.	Dev. %
ν(O–H) oxime	3317	3421	3.14
ν(C–H) aromatic	3064	3064	0.00
ν(C–H) aliphatic	2974	2974	0.00
ν(C=N) imine	1676	1676	0.00
ν(C=N) oxime	1660	1660	0.00
ν(C=N) pyridine	1593	1593	0.00
ν(C=N) thiazole	1579	1579	0.00
ν(C=C) aromatic	1521	1521	0.00
ν(N–O) oxime	—	1150	—
ν(C–S) thiazole	—	1080	—

neglect of intermolecular hydrogen bonding in the gas-phase model [77]. Table 11 presents the comparison.

MEP and Charge Distribution

The MEP map (Fig. 21) and Table 12 computed on the 0.001 e/bohr³ isodensity surface [66], identified the four nitrogen atoms (two imine, pyridine, and thiazole) as the most nucleophilic sites (negative potential regions), supporting the proposed N_4-tetradentate coordination mode in the [Au(SBTOx-OH)]Cl_3 complex. The sulfur atom of the thiazole ring exhibited a partial positive potential (+0.267 e by Mulliken analysis as shown in Fig. 22 and Table 12 [67]), while the oxime oxygen (−0.162 e) was confirmed as non-coordinating, consistent with the unchanged ν(O–H) frequency upon complexation. The computed dipole moment of 1.77 Debye reflects the moderate polarity of the molecule, directed from the oxime toward the thiazole terminus.

In summary, the DFT calculations at the B3LYP/6-311++G(d,p) level provided a comprehensive electronic and spectroscopic characterization of SBTOx-OH fully consistent with the experimental data. The HOMO–LUMO gap of 3.6754 eV and the electrophilicity index of 4.3185 eV confirm the moderate reactivity and strong electrophilic

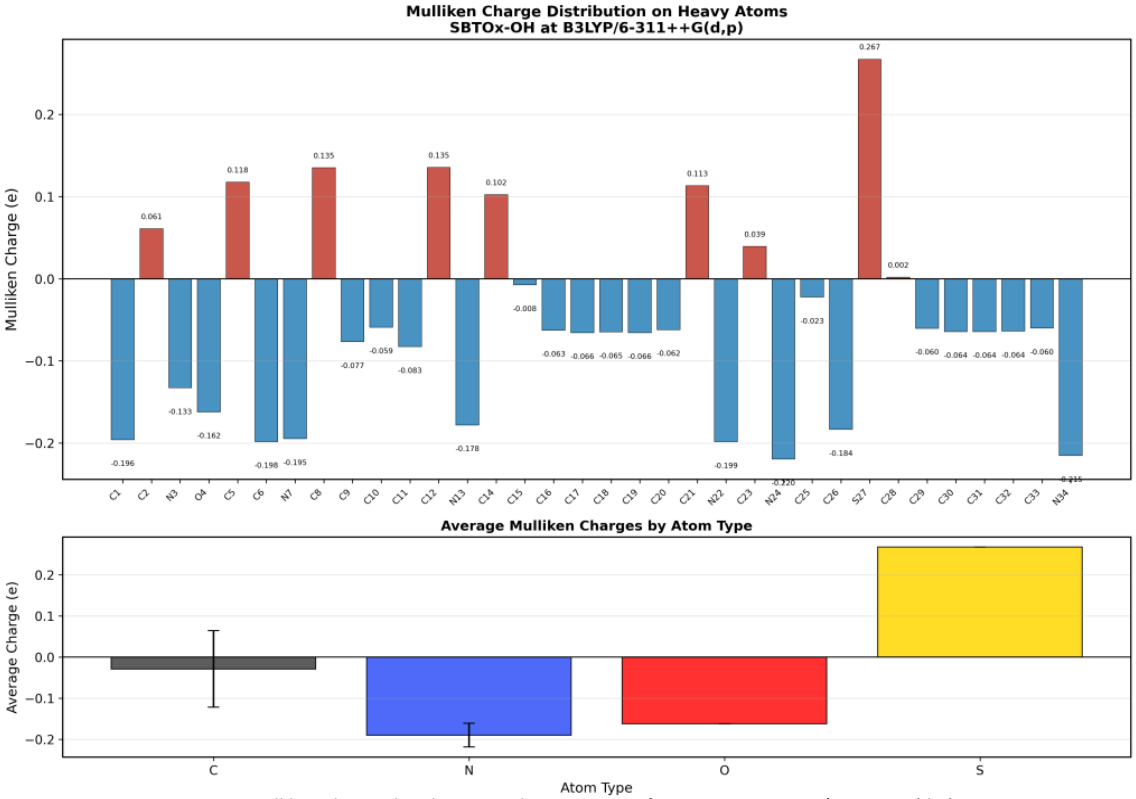

Fig. 22. Mulliken charge distribution on heavy atoms of SBTOx-OH at B3LYP/6-311++G(d,p).

Table 12. Selected Mulliken Atomic Charges (e) for Key Atoms in SBTOx-OH.

Atom	Type	Charge (e)	Role
N3	Oxime (=N–OH)	−0.133	H-bond acceptor
N7	Imine (C=N)	−0.195	Donor to Au^{3+}
N13	Pyridine	−0.178	Donor to Au^{3+}
N22	Imine (C=N)	−0.199	Donor to Au^{3+}
N24	Thiazole	−0.220	Donor to Au^{3+}
O4	Oxime (N–OH)	−0.162	Non-coordinating
S27	Thiazole	+0.267	Partial positive

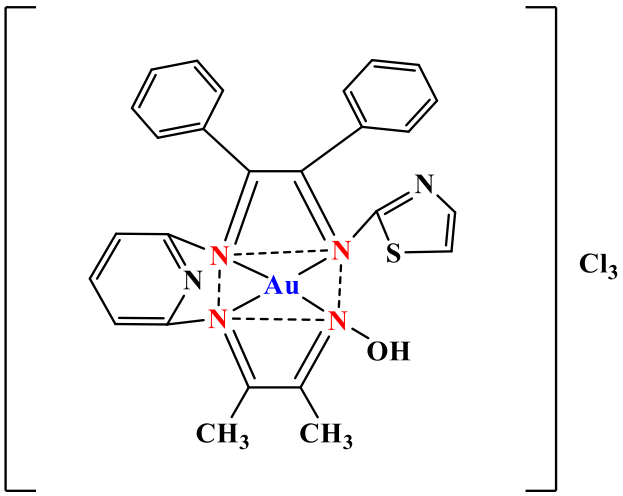

Fig. 23. The proposed chemical structure formula of the Gold(III) complex.

character of the ligand. The MEP analysis and Mulliken charges confirm the ligand's suitability as a tetradentate N-donor chelator for Au(III), and the high electrophilicity may contribute to the observed cytotoxic activity against MCF-7 cells [75,78].

CONCLUSION

Spectroscopic methods (infrared spectroscopy, ultraviolet spectroscopy, and nuclear magnetic resonance spectroscopy), atomic absorption, in addition to FESEM and XRD techniques, as well as physical methods (melting point, molar conductivity, elemental microanalysis) were employed to confirm the structure of the resulting ligand (SBTOx-OH) and its gold(III) complex. The infrared spectrum demonstrated that the ligand coordinates with the gold(III) ion through the nitrogen atoms of the four azomethine groups (C=N), acting as a tetradentate ligand, while the hydroxyl group of the oxime remained uncoordinated as confirmed by the unchanged ν(O–H) band. The molar conductivity value (131.27 ohm^{-1} cm^2 mol^{-1}) is consistent with a 1:3 electrolyte, supporting the formulation $[Au(SBTOx\text{-}OH)]Cl_3$ in which the three chloride ions are located outside the coordination sphere. These measurements, together with the UV-Vis and magnetic susceptibility data, are consistent with the proposed square planar geometry for the gold(III) complex, though definitive structural confirmation would require single-crystal X-ray diffraction. In the cytotoxicity assays conducted on the ligand (SBTOx-OH) and the gold complex against both breast cancer cells (MCF-7) and normal human dermal fibroblast cells (HdFn), the free ligand exhibited a higher IC_{50} value (122.86 µg/mL) against MCF-7 compared to the gold complex (111.2 µg/mL) indicating marginally stronger cytotoxic potency; however, the selectivity index of the gold complex (SI ≈ 1.16) was modest compared to the free ligand (SI = 3.35), indicating that the ligand possesses a significantly better therapeutic window. These findings position the free ligand as a preliminary lead-like scaffold exhibiting moderate cytotoxic activity and favorable selectivity, which warrants further structural optimization, mechanism-of-action studies, and expanded biological evaluation across multiple cell lines to assess its therapeutic potential.

CONFLICT OF INTEREST

The authors declare that there is no conflict of interests regarding the publication of this manuscript.

REFERENCES

1. Systematic Review on Thiazole Compounds as Nanoparticles: Chemistry, Synthesis, Antimicrobial Activities, Therapeutic Investigation. Nanosistemi, Nanomateriali, Nanotehnologii. 2023;21(1).
2. Khan K, Ahmad A, Ambreen N, Amyn A, Perveen S, Khan S, et al. Schiff Bases of 3-Formylchromones as Antibacterial, Antifungal, and Phytotoxic Agents (Supplementry Table).

Letters in Drug Design and Discovery. 2009;6(5):363-373.
3. Maradiya HR, Patel VS. Synthesis and Application of Disperse Dyes Based on 2-Aminothiazole Derivatives. ChemInform. 2003;34(45).
4. Bell AT. The Impact of Nanoscience on Heterogeneous Catalysis. Science. 2003;299(5613):1688-1691.
5. Zhang B, Liu D, Sun Y, Zhang Y, Feng J, Yu F. Preparation of Thiazole-2-thiones through TBPB-Promoted Oxidative Cascade Cyclization of Enaminones with Elemental Sulfur. Org Lett. 2021;23(8):3076-3082.
6. International Journal of Chemical Synthesis and Chemical Reactions.
7. Charef N, Sebti F, Arrar L, Djarmouni M, Boussoualim N, Baghiani A, et al. Synthesis, characterization, X-ray structures, and biological activity of some metal complexes of the Schiff base 2,2′-(((azanediylbis(propane-3,1-diyl))bis(azanylylidene))bis(methanylylidene))diphenol. Polyhedron. 2015;85:450-456.
8. Tadele KT, Tsega TW. Schiff Bases and their Metal Complexes as Potential Anticancer Candidates: A Review of Recent Works. Anticancer Agents Med Chem. 2019;19(15):1786-1795.
9. Sathiyaraj S, Ayyannan G, Jayabalakrishnan C. Synthesis, spectral, dna binding and cleavage properties of ruthenium(II) Schiff base complexes containing PPh3/AsPh3 as co-ligands. J Serb Chem Soc. 2014;79(2):151-165.
10. Mobinikhaledi A, Foroughifar N, Kalhor M. An efficient synthesis of Schiff bases containing benzimidazole moiety catalyzed by transition metal nitrates. Turkish Journal of Chemistry. 2010.
11. Bachmann WE, Cava MP, Dreiding AS. The Conversion of Primary Amines to Carbonyl Compounds by a Chloromine Degradation 1. Journal of the American Chemical Society. 1954;76(21):5554-5555.
12. Lettré H, Knof L. Über Azasterine, II. 6-Aza-cholesterin und Derivate. Chem Ber. 1960;93(12):2860-2864.
13. da Silva CM, da Silva DL, Modolo LV, Alves RB, de Resende MA, Martins CVB, et al. Schiff bases: A short review of their antimicrobial activities. Journal of Advanced Research. 2011;2(1):1-8.
14. Pahonțu E, Ilieș D-C, Shova S, Paraschivescu C, Badea M, Gulea A, et al. Synthesis, Characterization, Crystal Structure and Antimicrobial Activity of Copper(II) Complexes with the Schiff Base Derived from 2-Hydroxy-4-Methoxybenzaldehyde. Molecules. 2015;20(4):5771-5792.
15. Reddy GNR, Kondaiah S, Setty KN, Rao RM, Ramulu JS. Synthesis, Structural Characterization and Anti-bacterial Activity of some Novel Schiff base Ligands and their Vanadium (IV) Metal Complexes. Oriental Journal Of Chemistry. 2012;28(4):1673-1683.
16. Rangappa MM, Keshavayya J, Murali Krishna P, Rajesh K. Transition metal complexes of ligand 4-imino-3-[(4,5,6,7-tetrahydro-1,3-benzothiazol-2-yl)diazenyl]-4H pyrimido[2,1-b][1,3]benzothiazol-2-ol containing benzothiazole moiety: Synthesis, spectroscopic characterization and biological evaluation. Inorg Chem Commun. 2021;127:108524.
17. Acharya R, Chacko S, Bose P, Lapenna A, Pattanayak SP. Structure Based Multitargeted Molecular Docking Analysis of Selected Furanocoumarins against Breast Cancer. Sci Rep. 2019;9(1).
18. Vilar S, Cozza G, Moro S. Medicinal Chemistry and the Molecular Operating Environment (MOE): Application of QSAR and Molecular Docking to Drug Discovery. Curr Top Med Chem. 2008;8(18):1555-1572.
19. Pagadala NS, Syed K, Tuszynski J. Software for molecular docking: a review. Biophys Rev. 2017;9(2):91-102.
20. Halgren TA. Merck molecular force field. I. Basis, form, scope, parameterization, and performance of MMFF94. J Comput Chem. 1996;17(5-6):490-519.
21. Bento AP, Hersey A, Félix E, Landrum G, Gaulton A, Atkinson F, et al. An open source chemical structure curation pipeline using RDKit. J Cheminform. 2020;12(1).
22. Riniker S, Landrum GA. Better Informed Distance Geometry: Using What We Know To Improve Conformation Generation. J Chem Inf Model. 2015;55(12):2562-2574.
23. Halgren TA. Merck molecular force field. III. Molecular geometries and vibrational frequencies for MMFF94. J Comput Chem. 1996;17(5-6):553-586.
24. Becke AD. Density-functional thermochemistry. III. The role of exact exchange. The Journal of Chemical Physics. 1993;98(7):5648-5652.
25. Lee C, Yang W, Parr RG. Development of the Colle-Salvetti correlation-energy formula into a functional of the electron density. Physical Review B. 1988;37(2):785-789.
26. Stephens PJ, Devlin FJ, Chabalowski CF, Frisch MJ. Ab Initio Calculation of Vibrational Absorption and Circular Dichroism Spectra Using Density Functional Force Fields. The Journal of Physical Chemistry. 1994;98(45):11623-11627.
27. Krishnan R, Binkley JS, Seeger R, Pople JA. Self-consistent molecular orbital methods. XX. A basis set for correlated wave functions. The Journal of Chemical Physics. 1980;72(1):650-654.
28. Kohn W, Sham LJ. Self-Consistent Equations Including Exchange and Correlation Effects. Phys Rev. 1965;140(4A):A1133-A1138.
29. Koopmans T. Über die Zuordnung von Wellenfunktionen und Eigenwerten zu den Einzelnen Elektronen Eines Atoms. Physica. 1934;1(1-6):104-113.
30. Parr RG, Pearson RG. Absolute hardness: companion parameter to absolute electronegativity. Journal of the American Chemical Society. 1983;105(26):7512-7516.
31. Yang W, Parr RG. Hardness, softness, and the fukui function in the electronic theory of metals and catalysis. Proceedings of the National Academy of Sciences. 1985;82(20):6723-6726.
32. Parr RG, Szentpály Lv, Liu S. Electrophilicity Index. Journal of the American Chemical Society. 1999;121(9):1922-1924.
33. Stratmann RE, Scuseria GE, Frisch MJ. An efficient implementation of time-dependent density-functional theory for the calculation of excitation energies of large molecules. The Journal of Chemical Physics. 1998;109(19):8218-8224.
34. Merrick JP, Moran D, Radom L. An Evaluation of Harmonic Vibrational Frequency Scale Factors. The Journal of Physical Chemistry A. 2007;111(45):11683-11700.
35. Politzer P, Murray JS. Relationships of Electrostatic Potentials to Intrinsic Molecular Properties. Theoretical and Computational Chemistry: Elsevier; 1996. p. 649-660. http://dx.doi.org/10.1016/s1380-7323(96)80056-2
36. Mulliken RS. Electronic Population Analysis on LCAO–MO Molecular Wave Functions. I. The Journal of Chemical Physics. 1955;23(10):1833-1840.
37. McGraw ML, Reilly LT, Clarke RW, Cavallo L, Falivene L, Chen EYX. Mechanism of Spatial and Temporal Control in Precision Cyclic Vinyl Polymer Synthesis by Lewis Pair

Polymerization. Angew Chem Int Ed. 2022;61(15).
38. Benassi E, Fan H. Quantitative characterisation of the ring normal modes. Pyridine as a study case. Spectrochimica Acta Part A: Molecular and Biomolecular Spectroscopy. 2021;246:119026.
39. Yasir AF, Jamel HO. Synthesis of a New DPTYEAP Ligand and Its Complexes with Their Assessments on Physical Properties, Antioxidant, and Biological Potential to Treat Breast Cancer. Indonesian Journal of Chemistry. 2023;23(3):796.
40. Sumathi T, Nithya R, Kamatchi S, Ramanathan P. Synthesis, Spectral Analysis, DFT and Molecular docking studies of Some Novel Oxime Derivatives. Chemical Physics Impact. 2024;8:100583.
41. Nelson C, Schmidt AB, Adelabu I, Nantogma S, Dilday S, Volya N, et al. RASER for Increased Spectral Resolution in Carbon-13 NMR. Anal Chem. 2025;97(16):8738-8746.
42. Camellia FK, Ashrafuzzaman M, Islam MN, Banu LA, Zahan MK-E. Isoniazid Derived Schiff Base Metal Complexes: Synthesis, Characterization, Thermal Stability, Antibacterial and Antioxidant Activity Study. Asian Journal of Chemical Sciences. 2022:23-36.
43. Aziz DM, Hassan SA, Hamad OQ. Azo-azomethine complex activity and sensor potential toward Ca(II) ion in life samples: The spectroscopic and morphological studies. J Mol Struct. 2023;1293:136204.
44. second Conference CoAS, Abdulridha Hussein A, Obaid Jamel H. A novel imine-oxime ligand and its pd (II) complex: Synthesis, nano properties and anti-cancer evaluation. Bulletin of Pharmaceutical Sciences Assiut University. 2025;0(0):0-0.
45. Asemani M, Rabbani AR. Detailed FTIR spectroscopy characterization of crude oil extracted asphaltenes: Curve resolve of overlapping bands. Journal of Petroleum Science and Engineering. 2020;185:106618.
46. Ma F, Huang A-m, Zhang S-f, Zhou Q, Zhang Q-h. Identification of three Diospysros species using FT-IR and 2DCOS-IR. J Mol Struct. 2020;1220:128709.
47. Zhao Y, Shi T, Shang J, Ding L, Cao X, Chen C, et al. Rapid proton exchange between surface bridging hydroxyls and adsorbed molecules on TiO2. Applied Catalysis B: Environmental. 2020;277:119234.
48. Aburumman D, Marashdeh A. Theoretical Study of Substituted Aryl Isocyanide, Alkyl Isocyanide Ligands of Gold(I) Complexes for Focused Electron Beam Induced Deposition (FEBID). SSRN Electronic Journal. 2025.
49. Mohsen Q, S. Refat M. Synthesis, and spectroscopic characterizations of gold(III) complexes containing nitrogen-heterocycle based pyridine derivatives as a biomolecular chelates. Bull Chem Soc Ethiop. 2024;39(1):111-121.
50. Cai C, Wang G, Bai X, Xu D, Yan C, Yang Y. Optimizing carboxylated nanocellulose preparation: A kinetic and mechanistic study on the enhancement of TEMPO-mediated oxidation via swelling treatment. Int J Biol Macromol. 2024;274:133342.
51. Al-Daffay RKH, Al-Hamdani AAS. Synthesis, Characterization, and Thermal Analysis of a New Acidicazo Ligand's Metal Complexes. Baghdad Science Journal. 2023;20(1):0121.
52. Munawar S, Khalid MH, Anwar H, Jamil Y. Absorption and fluorescence properties of transition metal compounds. Modern Luminescence from Fundamental Concepts to Materials and Applications, Volume 2: Elsevier; 2025. p. 3-29. http://dx.doi.org/10.1016/b978-0-323-88662-8.00001-2
53. Lord N. Visual complex analysis. The Mathematical Gazette. 2024;108(573):561-563.
54. Zhao MM, Yang Y, Du N, Zhu YY, Ren P, Yen F. Determining the chemical composition of diamagnetic mixed solids via measurements of their magnetic susceptibility. Journal of Materials Chemistry C. 2024;12(16):5877-5885.
55. Elkanzi NAA, Hrichi H, Salah H, Albqmi M, M.Ali A, Abdou A. Synthesis, physicochemical properties, biological, molecular docking and DFT investigation of Fe(III), Co(II), Ni(II), Cu(II) and Zn(II) complexes of the 4-[(5-oxo-4,5-dihydro-1,3-thiazol-2-yl)hydrazono]methyl}phenyl 4-methylbenzenesulfonate Schiff-base ligand. Polyhedron. 2023;230:116219.
56. Unruh DK, Forbes TZ. X-ray Diffraction Techniques. Analytical Geomicrobiology: Cambridge University Press; 2019. p. 215-237. http://dx.doi.org/10.1017/9781107707399.009
57. Türkmenoğlu M, Yıldırım ST, Altay A, Türkmenoğlu B. Synthesis, Characterization, Investigation of Anticancer Activity and Molecular Docking Studies of N_2O_2 Type Schiff Base Ligand and Metal Complexes. ChemistrySelect. 2024;9(4).
58. Ferretti C, Chiaverini L, Poma N, Dalli A, Di Leo R, Rindi L, et al. Antimicrobial and Antibiofilm Activity of Auranofin and Its Two Derivatives Bearing Naproxen and Acetylcysteine as Ligands Against Staphylococci. Antibiotics. 2025;14(2):118.
59. Ghasemi L, Esfahani MH, Sahebi U, Divsalar A, Abbasi A, Behzad M. Experimental and molecular docking investigation of anticancer activity of new mixed-ligand Schiff base complexes against human colorectal (HCT116), lung (A549) and breast (MCF7) carcinoma cell lines. J Mol Struct. 2023;1294:136568.
60. Abou Melha KSA, Al-Hazmi GAA, Refat MS. Synthesis of Nano-Metric Gold Complexes with New Schiff Bases Derived from 4-Aminoantipyrene, Their Structures and Anticancer Activity. Russ J Gen Chem. 2017;87(12):3043-3051.
61. Ćwiklińska-Jurkowska M, Wiese-Szadkowska M, Janciauskiene S, Paprocka R. Disparities in Cisplatin-Induced Cytotoxicity—A Meta-Analysis of Selected Cancer Cell Lines. Molecules. 2023;28(15):5761.
62. Uddin E, Sardar MN, Reza MS, Hasan MS, Talukder MT, Hoque MM, et al. Emerging pharmaceutically active drugs: synthesis and pharmacology of Schiff base ligands with their metal complexes. Discover Chemistry. 2025;2(1).
63. Abdel-Rahman LH, Abdelghani AA, AlObaid AA, El-ezz DA, Warad I, Shehata MR, et al. Novel Bromo and methoxy substituted Schiff base complexes of Mn(II), Fe(III), and Cr(III) for anticancer, antimicrobial, docking, and ADMET studies. Sci Rep. 2023;13(1).
64. Samaszko-Fiertek J, Dmochowska B, Madaj J. Anticancer Activity of Schiff Base Metal Complexes Against MCF-7 Breast Cancer Cell Line. Int J Mol Sci. 2026;27(2):678.
65. Kumar S, Arora A, Maikhuri VK, Chaudhary A, Kumar R, Parmar VS, et al. Advances in chromone-based copper(ii) Schiff base complexes: synthesis, characterization, and versatile applications in pharmacology and biomimetic catalysis. RSC Advances. 2024;14(24):17102-17139.
66. Elsamra RMI, Masoud MS, Ramadan AM. Designing metal chelates of halogenated sulfonamide Schiff bases as potent nonplatinum anticancer drugs using spectroscopic, molecular docking and biological studies. Sci Rep. 2022;12(1).
67. Refat MS, El-Sayed MY, Adam AMA. Cu(II), Co(II) and

Ni(II) complexes of new Schiff base ligand: Synthesis, thermal and spectroscopic characterizations. J Mol Struct. 2013;1038:62-72.
68. Abu-Dief AM, Mohamed IMA. A review on versatile applications of transition metal complexes incorporating Schiff bases. Beni-Suef University Journal of Basic and Applied Sciences. 2015;4(2):119-133.
69. Fukui K, Yonezawa T, Shingu H. A Molecular Orbital Theory of Reactivity in Aromatic Hydrocarbons. The Journal of Chemical Physics. 1952;20(4):722-725.
70. Chattaraj PK, Sarkar U, Roy DR. Electrophilicity Index. Chem Rev. 2006;106(6):2065-2091.
71. Geerlings P, De Proft F, Langenaeker W. Conceptual Density Functional Theory. Chem Rev. 2003;103(5):1793-1874.
72. Pearson RG. Hard and Soft Acids and Bases. Journal of the American Chemical Society. 1963;85(22):3533-3539.
73. Chattaraj PK, Giri S, Duley S. Update 2 of: Electrophilicity Index. Chem Rev. 2011;111(2):PR43-PR75.
74. Umar N, Lawal MM, Soliman ME. DFT Study of the Structural and Electronic Properties of Selected Organogold(III) Compounds with Characteristic Anticancer Activity. Russian Journal of Physical Chemistry A. 2019;93(8):1543-1558.
75. Jacquemin D, Wathelet V, Perpète EA, Adamo C. Extensive TD-DFT Benchmark: Singlet-Excited States of Organic Molecules. J Chem Theory Comput. 2009;5(9):2420-2435.
76. Scott AP, Radom L. Harmonic Vibrational Frequencies: An Evaluation of Hartree−Fock, Møller−Plesset, Quadratic Configuration Interaction, Density Functional Theory, and Semiempirical Scale Factors. The Journal of Physical Chemistry. 1996;100(41):16502-16513.
77. Ott I. On the medicinal chemistry of gold complexes as anticancer drugs. Coord Chem Rev. 2009;253(11-12):1670-1681.